Chinese Chemical Letters 34 (2023) 107556

Contents lists available at ScienceDirect

Chinese Chemical Letters

journal homepage: www.elsevier.com/locate/cclet

Highly stable metal halides Cs_2ZnX_4 (X = Cl, Br) with Sn^{2+} as dopants for efficient deep-red photoluminescence

Yan Zhang[1], Lei Zhou[1], Lei Zhang, Wei Luo, Wei Shen, Ming Li, Rongxing He*

Key Laboratory of Luminescence Analysis and Molecular Sensing (Southwest University), Ministry of Education, College of Chemistry and Chemical Engineering, Southwest University, Chongqing 400715, China

ARTICLE INFO

Article history:
Received 7 February 2022
Revised 26 April 2022
Accepted 21 May 2022
Available online 26 May 2022

Keywords:
Lead-free metal halides
Deep-red emission
Photoluminescence
High efficiency
Stability

ABSTRACT

The development of deep-red emitting lead-free metal-halide perovskites with high photoluminescence quantum yields (PLQYs) and outstanding stability remains a major challenge for displays and deep-tissue bioimaging. In this work, we report a facile and convenient solvothermal method to synthesize metal halides Cs_2ZnX_4 (X = Cl, Br) that however is PL innert at room temperature. Upon composition engineering utilizing Sn^{2+} as the dopant, the resulting Cs_2ZnCl_4:Sn not only emits strong deep-red PL peaked at 700 nm with the highest 99.4% PLQY among the similar materials so far, but also exhibits excellent structure stability in air (PLQY remains 96% after one year exposure to the atmosphere). Detailed experimental characterizations and theoretical calculations reveal that the deep-red emission stems from self-trapped excitons induced by the Sn^{2+} dopant. Particularly, triplet emission ($^3P_2 \rightarrow {}^1S_0$) from Sn-$5s^2$ orbitals has been observed at low temperature due to the break of parity-forbidden transition. This work provides an important guidance for the development of deep-red light-emitting materials with low price, high efficiency and excellent stability.

In the past few years, metal halide perovskites as luminescent materials have been widely studied because of their intriguing optoelectronic properties, including spectral tenability and high photoluminescence quantum yields (PLQYs) [1–4]. As the key to the development of next-generation displays, luminescent materials used as light-emitting diode (LED) are required not only to meet the color purity standards [5–7], but also to be low-cost and environmental friendliness [8–10]. Although great progresses have been achieved, the stability issue of perovskite is still a bottleneck [11–14]. Furthermore, lead-free metal halide perovskites with intense emission in deep-red spectral region (>660 nm) are very rare and remain great developing challenge [15,16], although they are more desirable for display, photoelectric detection, biological tissue imaging, and solid-state lighting [17–20]. Therefore, it is of great significance to develop environmental-friendly, stable metal halides with highly efficient deep-red luminescence.

Recently, the zero-dimensional (0D) metal halide Cs_2ZnCl_4 with wide bandgap of 4.2 eV and negligible luminescence [21] are once again becoming excellent candidates as active materials, because the luminescence properties of the materials used Cs_2ZnCl_4 as host can be greatly improved by doping strategy. For example, Cheng *et al.* [22] reported the Cu^+-doped blue emitting Cs_2ZnX_4 with PLQY of 65.3%. Su *et al.* [23] developed a near-infrared emission single crystal by incorporating Sb^{3+} into the Cs_2ZnCl_4 matrix with high PLQY of 69.9%. Although the PLQYs of these materials have been greatly enhanced compared with that of the pristine Cs_2ZnCl_4, their properties are still unsatisfactory, especially their structural stability towards humidity and thermal. Generally, there are many factors that determine the color tunability and PL efficiency of emitting materials, and the structure of luminescent center is a key one of them [24–28]. Because Cs_2ZnCl_4 has an orthorhombic crystal structure with disconnected $[ZnCl_4]^{2-}$ tetrahedrons, when the doped metal ion M^{x+} ($x = 1, 2$) is introduced into Cs_2ZnCl_4, a part of $[ZnCl_4]^{2-}$ tetrahedrons should be replaced by $[MCl_4]^{y-}$ ($y = 2, 3$) tetrahedrons, which is the origin of strong emission for doped Cs_2ZnCl_4 [22,29]. Previous reports [30,31] have demonstrated that the four coordinated Sn^{2+} ions are prone to induce red emission. When Sn^{2+} is used as a dopant, more luminescent centers associated with Sn^{2+} ions are introduced into the lattice of Cs_2ZnCl_4, which induces the generation of self-trapped excitons (STEs), ultimately leading to the formation of STE states with a deeper self-trapping depth [32–34]. Therefore, it is anticipated that the band gap of Cs_2ZnCl_4 would be reduced further and the deep-red emission can thus be realized by introducing Sn^{2+}

* Corresponding author.
E-mail address: herx@swu.edu.cn (R. He).
[1] These authors contributed equally to this work.

https://doi.org/10.1016/j.cclet.2022.05.070
1001-8417/

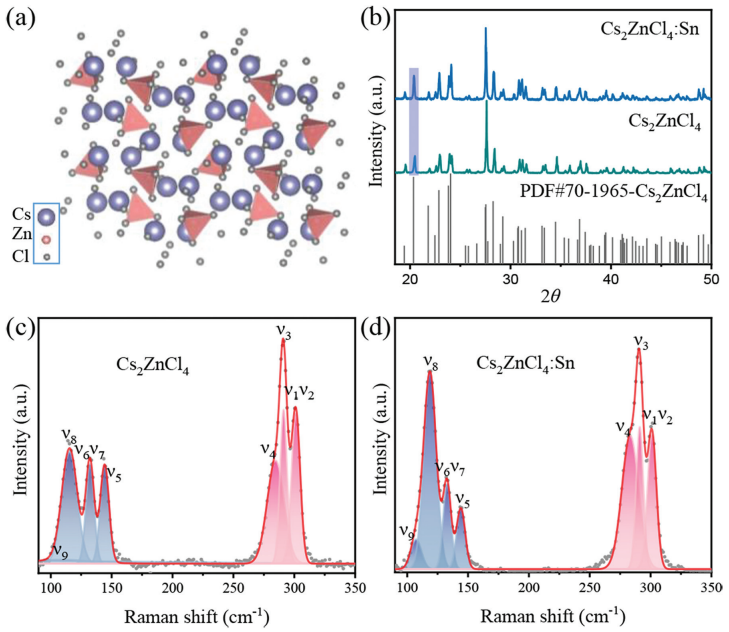

Fig. 1. (a) Crystal structure of Cs_2ZnCl_4. (b) PXRD diffractograms of Cs_2ZnCl_4 and Cs_2ZnCl_4:Sn. Raman spectrum of Cs_2ZnCl_4 (c) and Cs_2ZnCl_4:Sn (d).

into the lattice. The Sn^{2+}-doped Cs_2ZnCl_4 microcrystal has recently been developed by Wu and co-workers [35]. While its PL efficiency is unknown and the behind PL mechanism is poorly understood. For Cs_2ZnCl_4:Sn, the synthesis of its single crystals with lower defect densities is challenging. Thus, efficient deep-red emission is highly expected in Cs_2ZnCl_4:Sn single crystals, and the corresponding photophysical properties remain to be unveiled further.

Herein, we report a Sn^{2+}-doped 0D metal halide Cs_2ZnCl_4 (Cs_2ZnCl_4:Sn) with a broadband deep-red emission peaked at about 700 nm. By introducing Sn^{2+} into Cs_2ZnCl_4, an unprecedented improvement of PLQY (~99.4%) and outstanding stability (the PLQY of Cs_2ZnCl_4:Sn only decreases 4% when it is exposed to the air with relative humidity of 80% for 370 days) were realized. To the best of our knowledge, this is the best performance reported to date for any lead-free metal halides with deep-red emission. Detailed spectral characterizations and density functional theory (DFT) calculations revealed that the bright deep-red emission in Cs_2ZnCl_4:Sn originates from the STEs induced by the doped Sn^{2+} ion. For comparison, the Sn^{2+}-doped Cs_2ZnBr_4 (Cs_2ZnBr_4:Sn) emitting deep-red light (710 nm) was also synthesized using the same method, and its PLQY (~33.9%) and stability are also very prominent.

Cs_2ZnCl_4 and Sn^{2+}-doped Cs_2ZnCl_4 (*i.e.*, Cs_2ZnCl_4:Sn) single crystals were obtained through solvothermal reaction. The detailed synthesis and characterization are presented in Supporting information. It is reported that the crystal of Cs_2ZnCl_4 is orthorhombic space group *Pnam* [21]. The $[ZnCl_4]^{2-}$ tetrahedrons are isolated from each other by Cs^+ cations and thus form a 0D structure (Fig. 1a). Powder X-ray diffraction (PXRD) patterns of Cs_2ZnCl_4 and Cs_2ZnCl_4:Sn were measured and the main diffraction peaks were found to be unique to Cs_2ZnCl_4 (Fig. 1b). Compared with Cs_2ZnCl_4, the diffraction peak of Cs_2ZnCl_4:Sn at 20.5° (2θ) moves to a smaller angle, indicating that Sn^{2+} is incorporated into the Cs_2ZnCl_4 successfully. Moreover, Cs_2ZnBr_4 and Cs_2ZnBr_4:Sn were also synthesized and verified by PXRD (Fig. S1 in Supporting information). The oxidation state of Sn^{2+} was confirmed to be positively divalent by X-ray photoelectron spectroscopy (XPS) (Fig. S2 in Supporting information). As shown in Fig. S2d, the main bands located at 487 and 496 eV are derived from the Sn^{2+} $3d^5$ state. Inductively coupled plasma optical emission spectroscopy (ICP-OES) reveals the actual content of Sn^{2+} in various Cs_2ZnCl_4:Sn and Cs_2ZnBr_4:Sn samples. The results shown in Table S1 (Supporting information) unveil the actual Sn^{2+} content of the maximum feeding ratio samples for Cs_2ZnCl_4:Sn and Cs_2ZnBr_4:Sn is only 1.42% and 1.12%, respectively, implying that the feeding Sn^{2+} precursor was only partially embedded into the Cs_2ZnX_4 lattice. Moreover, the slight shift of the XRD peaks towards a small angle further demonstrates the incorporation of trace amounts of Sn^{2+} in Cs_2ZnX_4. Nevertheless, the photophysical properties of Cs_2ZnX_4 have been modulated greatly after Sn^{2+} doping, which will be discussed later. In this article, unless otherwise specified, the samples with the highest actual doping rate (*i.e.*, Cs_2ZnCl_4:1.42%Sn and Cs_2ZnBr_4:1.12%Sn) were chosen for all tests, and abbreviated as Cs_2ZnCl_4:Sn and Cs_2ZnBr_4:Sn for simplicity. To shed new light on the structural changes of doped samples, Raman spectra of Cs_2ZnCl_4 and Cs_2ZnCl_4:Sn were measured. As shown in Figs. 1c and d and Table S2 (Supporting information), the Raman peaks of Cs_2ZnCl_4 and Cs_2ZnCl_4:Sn are very similar, indicating that the introduction of Sn^{2+} does not destroy the lattice of Cs_2ZnCl_4. Here, the relative intensity and the positions of Zn-Cl stretching mode (ν_1-ν_4) and Cl-Zn-Cl bending mode (ν_5-ν_9) are changed slightly for Cs_2ZnCl_4:Sn due to the distortion of $[ZnCl_4]^{2-}$ tetrahedron after Sn^{2+} doping. The above analysis confirmed that Sn^{2+} was successfully doped into the lattice of Cs_2ZnCl_4 by substituting a small part of Zn^{2+}.

The optical properties of these materials were characterized by UV–vis absorption spectroscopy and PL spectroscopy. The solid-state UV–vis spectrum of Cs_2ZnCl_4 in Fig. 2a exhibits absorption below 400 nm, with an intense absorption peak at ~270 nm, indicating the negligible absorption in visible-light region. While a shoulder peak between 300 and 400 nm emerges after Sn^{2+} doping, which can be attributed to the absorption of $[SnCl_4]^{2-}$ tetrahedron, suggesting the successful embedding of Sn^{2+} in Cs_2ZnCl_4 [36]. As shown in Fig. 2b, an additional narrow-band peak (~350 nm) appears in the PL excitation (PLE) spectrum, which is the main feature of the red emission observed for the Sn^{2+}-doped materials [37,38]. Figs. 2b and c and Table S3 (Supporting information) provide the room-temperature PL properties of Cs_2ZnCl_4 with different Sn^{2+} content, revealing that the PLQY gradually increases with the increase of Sn^{2+} doping concentration. This is because

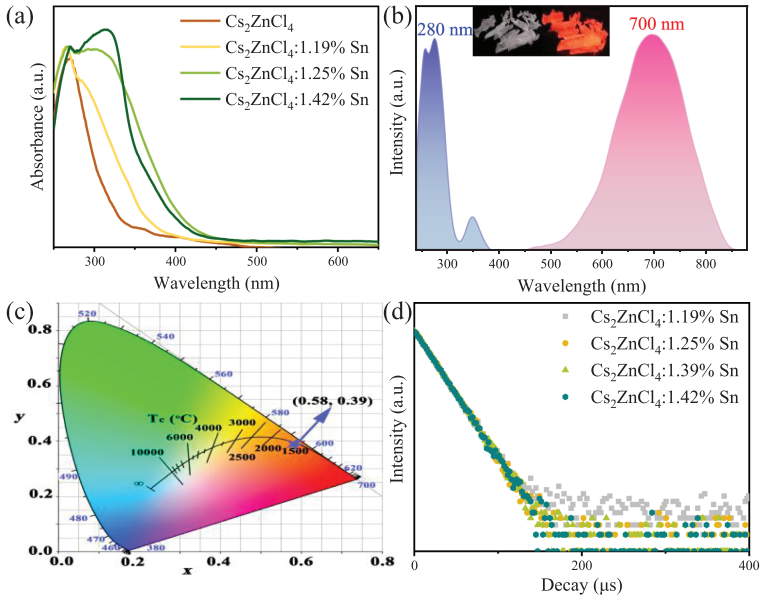

Fig. 2. (a) UV–vis absorption spectra of Cs_2ZnCl_4 and Cs_2ZnCl_4:Sn. (b) Room-temperature PL and PLE spectra of Cs_2ZnCl_4:Sn. (c) CIE chromaticity diagram of Cs_2ZnCl_4:Sn. (d) Room-temperature PL decay curves of Cs_2ZnCl_4:Sn.

that more luminescent centers associated with Sn^{2+} ions are introduced into the lattice of Cs_2ZnCl_4 and the optimum luminescent performance is obtained when the actual doping amount reaches $n_{Sn}:n_{Zn} = 1.42\%$. After that, impurity such as $CsSnCl_3$ was detected. For Cs_2ZnCl_4:1.42%Sn, a deep-red emission centered at ~700 nm is observed under 280 nm excitation with PLQY of 99.4% and the corresponding Commission Internationale de L'Eclairage (CIE) coordinates is (0.58, 0.39). It is worth adding that, to the best of our knowledge, such PLQY is the highest value of deep-red light among the reported metal-halide single crystals (Table S4 in Supporting information). The PL decay curves of Cs_2ZnCl_4:Sn with different Sn^{2+} concentrations were shown in Fig. 2d, and the corresponding data were presented in Table S5 (Supporting information). The average PL lifetime in Fig. 2d indicates a slight increase in PL lifetime with the increase of doping concentration, and the lifetime of Cs_2ZnCl_4:1.42%Sn is up to 18.3 μs. Such long lifetime, large Stokes shift and broad PL line suggest the deep-red emission might be from the radiative recombination of triplet STEs in $[SnCl_4]^{2-}$ tetrahedron, by inhibiting the non-radiative recombination in Cs_2ZnCl_4.

To gain more insight into the effect of Sn^{2+} on the photophysical properties of Cs_2ZnCl_4, first principle calculations were carried out. As displayed in Fig. 3a, the calculated energy bandgap of Cs_2ZnCl_4 is 4.62 eV, while that of Sn^{2+}-doped Cs_2ZnCl_4 is reduced to 3.42 eV (Fig. 3b), which is in agreement with the experimentally reduced trend of bandgap (4.15 eV for Cs_2ZnCl_4 and 3.58 eV for Cs_2ZnCl_4:Sn). It is worth noting that the calculated band structure of Sn-doped Cs_2ZnCl_4 is more flatter, compared to that of the undoped Cs_2ZnCl_4, suggesting the excited carriers are more localized after the incorporation of Sn^{2+}. Upon examining the projected density of states (DOS) (Fig. S3 in Supporting information), the resultant valence band maximum (VBM) of Cs_2ZnCl_4 is mainly composed of Cs-p, Zn-d and Cl-p orbitals, and the conduction band minimum (CBM) consists of Cs-d, Zn-s and Cl-p orbitals. Conversely, for Cs_2ZnCl_4:Sn, its VBM are mainly contributed by Sn-s and Cl-p orbitals, and CBM are mainly composed of Sn-p and Cl-p orbitals. This verifies that the embedded Sn^{2+} ions change the position of VBM and CBM of Cs_2ZnCl_4 and reduce the band gap, resulting in the deep-red emission in Sn^{2+}-doped Cs_2ZnCl_4. In addition, the calculated charge density (Figs. 3c and d) demonstrates that the carriers are delocalized in both VBM and CBM of Cs_2ZnCl_4, whereas those are localized in $[SnCl_4]^{2-}$ tetrahedrons in Sn^{2+}-doped Cs_2ZnCl_4, agreeing perfectly with the DOS results. The highly localized charge density induces a statically expressed distortion of the $[SnCl_4]^{2-}$ tetrahedrons due to the presence of stereoactive $5s^2$ lone pair in Sn^{2+} [33,39], which is conducive to the formation of STEs, and thereby leading to the broadband deep-red emission [40].

The radiative recombination in 0D metal halides can originate from many aspects, such as permanent defects, free excitons (FE) and STEs. To probe into the origin of the deep-red emission, PLE and PL spectra of Cs_2ZnCl_4:Sn monitored at different wavelengths were carried out, and the consistency of the peaks shown in Fig. S4 (Supporting information) indicates the deep-red emission origins from an identical excited states. Further, upon the excitation power dependent PL measurements, the PL intensity of deep-red emission for Cs_2ZnCl_4:Sn is linear with the excitation power (Fig. 4a), eliminating the possibility that the deep-red emission is resulted from permanent defects. In contrast to FE emission that typically features with narrow PL band, small Stokes shifts and short lifetime is at nanosecond level, the PL spectrum of Sn^{2+}-doped Cs_2ZnCl_4 exhibits an ultra-broad full width at half maximum (FWHM) over 158 nm, a large Stokes shifts of 420 nm and a long PL lifetime up to 18.3 μs at room temperature, ruling out the possibility of FE emission. Combined with the calculated results, it can be reasonably speculated that the strong deep-red light of Cs_2ZnCl_4:Sn is originated from the triplet STE emission induced by Sn^{2+} dopant. To prove such conjecture, temperature-dependent PL spectra of Cs_2ZnCl_4:Sn was measured and the corresponding results were depicted in Fig. 4b and Fig. S5 (Supporting information). With the decrease of temperature, the maximum peak position gradually redshifts from 700 nm to 740 nm, as a result of the intense electron-phonon interaction [41]. Meanwhile, the PL intensity enhances with the decrease of temperature, suggesting the suppressed of nonradiative recombination. When the temperature is lower than 150 K, an obvious emission centered at 470 nm appears. Furthermore, as shown in Fig. S6 (Supporting information), the exciton binding energy (E_b) can be calculated with 190 meV, which is much higher than the thermal energy at room temperature (26 meV), providing a high probability of radiative combination in Cs_2ZnCl_4:Sn [42]. Meanwhile, the relationship between

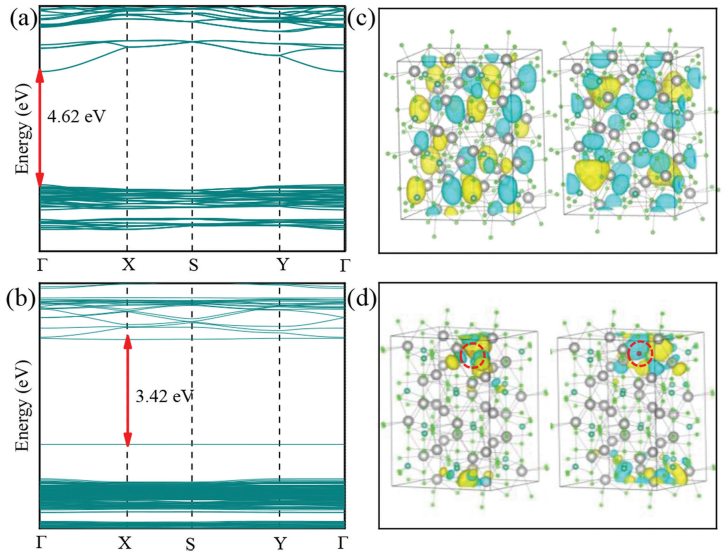

Fig. 3. Calculated band structure (a) and charge densities (VBM (left) and CBM (right)) (b) of Cs_2ZnCl_4. Calculated band structure (c) and charge densities (VBM (left) and CBM (right)) (d) of Cs_2ZnCl_4:Sn. The red circle denotes the doped Sn^{2+} ion.

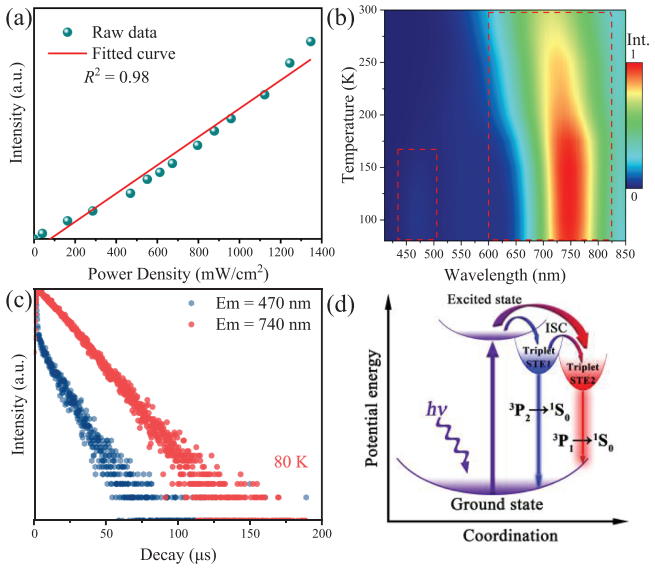

Fig. 4. (a) Dependence of the emission intensity at 700 nm of Cs_2ZnCl_4:Sn on the excitation power at 300 K ($\lambda_{ex} = 405$ nm). (b) Temperature-dependent PL spectra of Cs_2ZnCl_4:Sn. (c) PL decay curves of Cs_2ZnCl_4:Sn monitoring at 470 and 740 nm at 80 K ($\lambda_{ex} = 280$ nm). (d) Possible schematic diagram of the energy level of Cs_2ZnCl_4:Sn.

FWHM and temperature can be fitted, with a calculated Huang-Rhys factor (*S*) value of 62.6. Such a large *S* indicates the presence of a strong electron-phonon coupling effect in Cs_2ZnCl_4:Sn, which enables the formation of STEs and the broadening of PL band. To further probe into such emission, PL decay curves of Cs_2ZnCl_4:Sn were measured at 80 K (Fig. 4c and Table S6 in Supporting information). For comparison, the PL and PL decay lifetimes of Cs_2ZnCl_4 were also measured at the 80 K (Fig. S7 in Supporting information and Table S6). As shown in Table S6, the lifetime of the emission peak at 450 nm in Cs_2ZnCl_4 is 20 ns, much shorter than that of the emission peak at 470 nm in Cs_2ZnCl_4:Sn (10.33 μs), indicating that the emission at 470 nm also comes from the triplet STEs. For Sn^{2+} ions with $5s^2$ electronic configuration, its excited states can be composed of one singlet state ($^1P_1$) and three triplet states ($^3P_0$, $^3P_1$ and $^3P_2$), where the triplet states $^3P_0$, $^3P_1$ and $^3P_2$ can be further split due to spin-orbit interactions [43]. Undoubtedly, for Cs_2ZnCl_4:Sn, the emission peak at 740 nm in 80 K is attributed to the $^3P_1 \rightarrow {}^1S_0$ transition of Sn^{2+} ion [33], while the emission peak at 470 nm in 80 K may be assigned to the transition of $^3P_2 \rightarrow {}^1S_0$, as a result of the break of its forbidden nature at low temperature. In this situation, the crystal symmetry might be modulated or broken to convert the forbidden transition of $^3P_2 \rightarrow {}^1S_0$ to an allowed transition, thus further enabling the radiative emission, which has also been seen in bismuth-based materials [44].

Following the above results, the possible photophysical process of Cs_2ZnCl_4:Sn is illustrated in Fig. 4d. Briefly, upon the photoexcitation, electrons in the ground state are promoted to the excited states of $[SnCl_4]^{2-}$. And simultaneously, the highly localized electrons in excited states combining with the stereoactive $5s^2$ lone pair in Sn^{2+} induce structural distortion of $[SnCl_4]^{2-}$ polyhedron that further leads to the formation of STEs [45]. Then, the excitons will undergo an intersystem crossing (ISC) process to triplet STE state, where some of them are quickly self-trapped to relatively high energy states, enabling the blue light (~470 nm) emission, while the rest will transfer to low energy STE state, finally resulting in the highly efficient deep-red emission with a large Stokes shift and long lifetime.

To expand the scope of materials, Cs_2ZnBr_4:Sn was also synthesized and studied to uncover the effect of halogen on the PL properties, details of which can be found in Supporting information. Furthermore, as an excellent luminescent material, except for the outstanding luminescent efficiency, stability is also important for practical applications. As illustrated in Fig. S10a (Supporting information), the thermal stability of Cs_2ZnCl_4:Sn and Cs_2ZnBr_4:Sn was evaluated by thermogravimetry analysis (TGA), and the results reveal that both of the two materials are thermally stable up to 610 °C, indicating their excellent thermal stability that is extremely important for optoelectronic applications. Moreover, their humidity stability was also investigated. As shown in Fig. S10b (Supporting information), the XRD profiles of the two materials after exposing to the atmosphere (relative humidity > 80%) for one year exhibit almost no significant change compared with that of their freshly prepared samples, manifesting that both Cs_2ZnCl_4:Sn and Cs_2ZnBr_4:Sn are resistant to the humidity. Surprisingly, after exposing to atmosphere for one year, the PLQYs of Cs_2ZnCl_4:Sn decreased by only 4% (~30% for Cs_2ZnBr_4:Sn) compared with its initial values (Fig. S10c in Supporting information), further confirming

its excellent PL stability towards humidity. Generally, Sn^{2+} is unstable and can be easily oxidized to Sn^{4+} in air. In these two materials, the actual doping concentration of Sn^{2+} is extremely low (1.42% for Cs_2ZnCl_4:Sn and 1.12% for Cs_2ZnBr_4:Sn), thus Sn^{2+} is hardly oxidized in atmosphere with high humidity. Moreover, it is noteworthy that the Sn-X (X = Cl, Br) bond lengths here (2.28 Å for Cs_2ZnCl_4:Sn and 2.43 Å for Cs_2ZnBr_4:Sn) are significantly shorter than that in the previous reports (both Sn-Cl and Sn-Br are >2.5 Å) (Table S7 in Supporting information), which allows for stronger interactions between the Sn^{2+} ion and the halogen, resulting in the excellent stability of the studied materials.

In summary, we have successfully prepared the Sn^{2+}-doped 0D free-lead metal halides Cs_2ZnX_4:Sn (X = Cl, Br) with bright deep-red emission. The Cs_2ZnCl_4:Sn exhibits deep-red emission (700 nm) with ultra-high PLQY (99.4%) owing to the introduction of Sn^{2+} ions which can reduce the band gap of the native and induce triplet STE emission. Such a superior PL performance is attributed to the $5s^2$ lone pair electron expression of the Sn^{2+} ion. Most importantly, Cs_2ZnCl_4:Sn possess outstanding PL and structural stability, maintaining the PLQY under ambient air with relative humidity over 80% for more than 370 days. The present work not only sheds insight into the luminescent mechanism of Cs_2ZnX_4:Sn (X = Cl, Br), but also provides an efficient, stable and environment-friendly deep-red emitting material for promising optoelectronic devices and biological imaging.

Declaration of competing interest

The authors report no declarations of interest.

Acknowledgments

We acknowledge the financial supports from National Natural Science Foundation of China (Nos. 91741105, 22109130), Chongqing Municipal Natural Science Foundation (Nos. cstc2018jcyjAX0625, cstc2021jcyj-msxmX1180), and Program for Innovation Team Building at Institutions of Higher Education in Chongqing (No. CXTDX201601011).

Supplementary materials

Supplementary material associated with this article can be found, in the online version, at doi:10.1016/j.cclet.2022.05.070.

References

[1] C.C. Stoumpos, M.G. Kanatzidis, Acc. Chem. Res. 48 (2015) 2791–2802.
[2] K. Miyata, T.L. Atallah, X.Y. Zhu, Sci. Adv. 3 (2017) e1701469.
[3] Z. Xiao, Z. Song, Y. Yan, Adv. Mater. 31 (2019) e1803792.
[4] G. Zhou, B. Su, J. Huang, Q. Zhang, Z. Xia, Mater. Sci. Eng. R 141 (2020) 100548.
[5] Q. Wang, M. Lyu, M. Zhang, J.H. Yun, L. Wang, J. Mater. Chem. A 5 (2017) 902–909.
[6] H. Lian, Y. Li, K. Sharafudeen, et al., Adv. Mater. 32 (2020) 2070208.
[7] X. Li, B. Traoré, M. Kepenekian, et al., Chem. Mater. 33 (2021) 6206–6216.
[8] Z. Ma, L. Wang, X. Ji, X. Chen, Z. Shi, J. Phys. Chem. Lett. 11 (2020) 5517–5530.
[9] A.H. Slavney, T. Hu, A.M. Lindenberg, H.I. Karunadasa, J. Am. Chem. Soc. 138 (2016) 2138–2141.
[10] Q. Li, W. Wei, Z. Xue, et al., Chin. Chem. Lett. 33 (2022) 3203–3206.
[11] Z. Xiao, K.Z. Du, W. Meng, et al., J. Am. Chem. Soc. 139 (2017) 6054–6057.
[12] A. Biswas, R. Bakthavatsalam, V. Bahadur, et al., J. Mater. Chem. C 9 (2021) 4351–4358.
[13] B.A. Connor, R.I. Biega, L. Leppert, H.I. Karunadasa, Chem. Sci. 11 (2020) 7708–7715.
[14] H. Yang, Y. Guo, G. Liu, et al., Chin. Chem. Lett. 33 (2022) 537–540.
[15] C. Zhou, H. Lin, H. Shi, et al., Angew. Chem. Int. Ed. 57 (2018) 1021–1024.
[16] O. Nazarenko, M.R. Kotyrba, S. Yakunin, et al., J. Am. Chem. Soc. 140 (2018) 3850–3853.
[17] Q. Zhang, P. Yu, Y. Fan, et al., Angew. Chem. Int. Ed. 60 (2021) 3967–3973.
[18] C.H. Fan, P. Sun, T.H. Su, C.H. Cheng, Adv. Mater. 23 (2011) 2981–2985.
[19] J. Liu, Y. Geng, D. Li, et al., Adv. Mater. 32 (2020) e1906641.
[20] Y. Liu, Y. Zhang, X. Zhu, et al., Adv. Mater. 33 (2021) 2006010.
[21] N. Yahaba, M. Koshimizu, Y. Sun, et al., Appl. Phys. Express 7 (2014) 062602.
[22] P. Cheng, L. Feng, Y. Liu, et al., Angew. Chem. Int. Ed. 59 (2020) 21414–21418.
[23] B. Su, M. Li, E. Song, Z. Xia, Adv. Funct. Mater. 22 (2021) 2105316.
[24] T. Jiang, W. Ma, H. Zhang, et al., Adv. Funct. Mater. 31 (2021) 2009973.
[25] B. Su, G. Zhou, J. Huang, et al., Laser Photonics Rev. 15 (2021) 2000334.
[26] M.D. Smith, B.A. Connor, H.I. Karunadasa, Chem. Rev. 119 (2019) 3104–3139.
[27] G. Zhang, P. Dang, H. Xiao, et al., Adv. Optical Mater. 34 (2021) 2101637.
[28] Y. Miao, Y. Chen, H. Chen, X. Wang, Y. Zhao, Chem. Sci. 12 (2021) 7231–7247.
[29] L. Zhou, L. Zhang, H. Li, et al., Adv. Funct. Mater. 31 (2021) 2108561.
[30] L.J. Xu, S. Lee, X. Lin, et al., Angew. Chem. Int. Ed. 59 (2020) 14120–14123.
[31] L. Fan, K. Liu, Q. Zeng, et al., ACS Appl. Mater. Interfaces 13 (2021) 29835–29842.
[32] Q. Wei, Y. Ke, Z. Ning, Energy Environ. Mater. 3 (2020) 541–547.
[33] V. Morad, Y. Shynkarenko, S. Yakunin, et al., J. Am. Chem. Soc. 141 (2019) 9764–9768.
[34] L. Zhou, J.F. Liao, D.B. Kuang, Adv. Optical Mater. 9 (2021) 2100544.
[35] X. Wang, Q. Shen, Y. Chen, et al., Nanoscale 13 (2021) 15285–15291.
[36] L. Zhou, J.F. Liao, Z.G. Huang, et al., Angew. Chem. Int. Ed. 58 (2019) 15435–15440.
[37] A. Méndez, F. Ramos, R. Guerrero, E. Camarillo, U. Caldiño Garcıá, J. Lumin. 79 (1998) 269–274.
[38] G. Song, Z. Li, P. Gong, R.J. Xie, Z. Lin, Adv. Optical Mater. 9 (2021) 2002246.
[39] K.M. McCall, V. Morad, B.M. Benin, M.V. Kovalenko, ACS Materials Lett. 2 (2020) 1218–1232.
[40] X. Wang, W. Meng, W. Liao, et al., J. Phys. Chem. Lett. 10 (2019) 501–506.
[41] H. Peng, S. Yao, Y. Guo, et al., J. Phys. Chem. Lett. 11 (2020) 4703–4710.
[42] K. Xu, Q. Wei, H. Wang, et al., Nanoscale 14 (2022) 2248–2255.
[43] P. Fu, M. Huang, Y. Shang, et al., ACS Appl. Mater. Interfaces 10 (2018) 34363–34369.
[44] W. Zheng, R. Sun, Y. Liu, et al., ACS Appl. Mater. Interfaces 13 (2021) 6404–6410.
[45] Q. Wei, H. Li, Z. Ning, Trends Chem. 4 (2022) 1–4.